Numerical Analysis of Inclined Uplift Capacity of Suction Caisson in Sand

Sheikh Sharif Ahmed and Bipul Chandra Hawlader
Department of Civil Engineering, Faculty of Engineering and Applied Science
Memorial University of Newfoundland, St. John's, Newfoundland, Canada

Three-dimensional finite element (FE) analyses are conducted to calculate the pullout capacity of suction caisson subjected to oblique loadings. Two sets of FE analyses are performed using Abaqus FE software. In the first set, the sand around the caisson is modeled using the built-in Mohr-Coulomb model (MC) available in Abaqus where constant values of angle of internal friction (ϕ') and dilation (ψ) are defined. The effects of key variables, such as loading angle, mooring position and aspect ratio, on pullout capacity and rotation of the caisson are examined. A comparison between FE and centrifuge test results is also shown. The second set of analyses are performed using a modified Mohr-Coulomb model (MMC) where the pre-peak hardening, post-peak softening and effects of density and confining pressure on stress-strain behavior of dense sand are implemented using a user subroutine by varying ϕ' and ψ as a function of plastic shear strain and confining pressure. Comparing the failure surface development in the soil with increase in loading for two different models (MC and MMC) it is shown that the mobilized ϕ' and ψ varies along the failure planes if the MMC model is used, although the capacity of the caisson could be obtained even if appropriate values of constant ϕ' and ψ are used in the MC model.

KEY WORDS: Suction caisson; Abaqus/Explicit; Pullout force; Dense sand; Loading angle; Mooring position.

INTRODUCTION

Suction caissons (also known as suction anchors, suction piles or suction buckets) are a unique form of foundation/mooring system that have several advantages over traditional pile foundation and anchors. The main advantages include fast installation, elimination of the pile driving process, reduction in material costs and reusability. A suction caisson is a large diameter hollow cylinder, usually made of steel having top end closed and bottom end opened that is installed in soil by applying suction with pumping water out of caisson interior. Suction caissons are now widely being used in offshore industries for anchoring large offshore floating facilities to the seafloor. The pullout capacity of the caisson is one of the main concerns. The caissons are usually connected to the floating structures by a mooring line which is attached to a padeye on one side of the caisson.

The pullout behavior of suction caissons installed in both sand and clay is of great interest for oil and gas development industry because of their advantages over other conventional foundation systems. Previous studies mainly focused on caissons in clay. For example, Aubeny et al. (2003) presented a theoretical method to estimate the inclined load capacity of suction caissons based on an upper bound plasticity formulation for clay. Cao et al. (2002a, b & 2003) conducted centrifuge tests and FE analyses for caissons in clay. Similarly, FE analyses have been performed using various soil constitutive models, including Cam Clay and MIT-E3 models, to understand the response of caissons in clay (e.g. Sukumaran et al., 1999; Handayanu et al., 2000; Zdravkovic et al., 2001).

Limited number of research is available in the literature to estimate the pullout capacity of suction caissons in sand. The mechanisms involved in the installation of a caisson in sand are different from that of in clay. In sand, the seepage due to applied suction plays a significant role. The installation issues of suction caisson in sand and sand/silt layers have been described by Houlsby and Byrne (2005a & b) and Tran et al. (2007). Some centrifuge tests have been conducted in the past to understand the pullout behavior of caisson in sand (e.g. Allersma et al., 2000; Lee et al., 2003; Kim et al., 2005; Jones et al. 2007; Kim et al., 2009; Kim et al., 2010; Bang et al., 2011; Jang and Kim 2013). Bang et al. (2011) reported a series of centrifuge tests at 100g on a model suction caisson in medium dense sand to evaluate the pullout capacities. More recently, Gao et al. (2013) conducted model tests to evaluate the pullout capacity of suction caisson in medium dense sand and reported the effects of load inclination angle, mooring position and aspect ratio.

Numerical modeling of suction caisson in sand is very limited. Deng and Carter (2000) conducted FE analyses of suction caisson in sand assuming axisymmetric loading conditions using the AFENA FE software package and Mohr-Coulomb soil model. Iftekharuzzaman and Hawlader (2012) conducted three-dimensional FE analysis using Abaqus/Standard FE software, where they encountered some mesh distortion issues at large displacement.

In this study, three-dimensional FE modeling of suction caisson is performed to evaluate the pullout capacities at different load inclination angles and mooring positions in dense sand. In the first part of the paper, FE analyses are conducted using the built-in Mohr-Coulomb model available in Abaqus where ϕ' and ψ are constant. A total of 60 cases are analyzed to determine the pullout capacity of the caisson. A parametric study is also conducted to evaluate the effects of length/diameter ratio on pullout capacity. The finite element results are compared with centrifuge test results available in literature. In the second part, a set of FE analyses are presented using a modified Mohr-Coulomb model in which the stress-strain behavior of dense sand as observed in laboratory tests is incorporated.

PROBLEM DEFINITION

A suction caisson of length L and diameter D installed in dense sand is simulated in this study. During the installation, the soil in the vicinity of the suction caisson can be disturbed. However, the effects of disturbance on capacity are not considered in this study, instead the simulations are performed for a wished-in-place suction caisson. The caisson is loaded at the five padeye locations shown in Fig. 1 (a) at different angle θ with the horizontal (Fig. 1b). The sign convention used for displacement and rotation of the caisson is shown in Fig. 1(c).

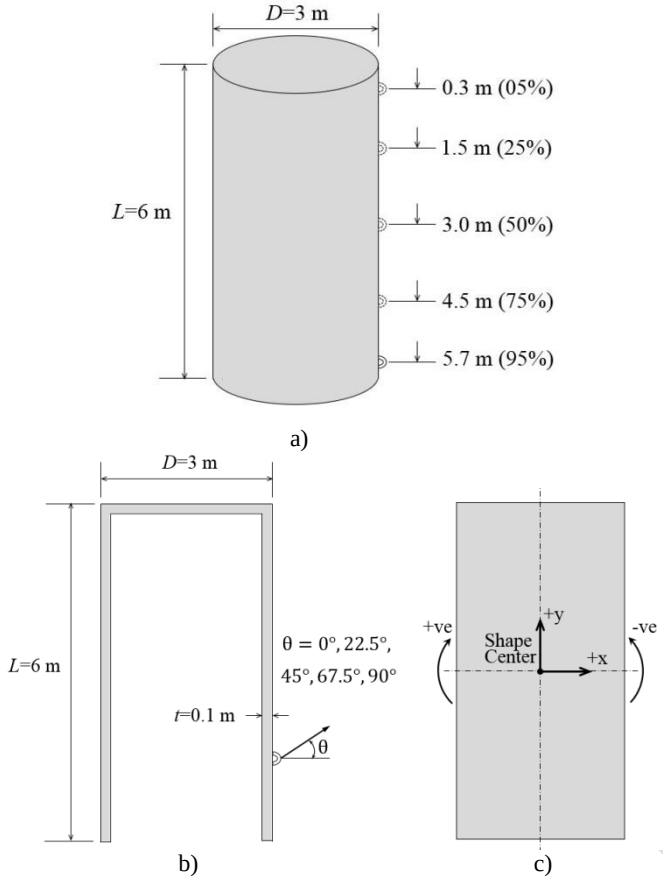

Fig. 1. Problem definition: a) padeye position, b) loading angle, c) sign convention for displacement and rotation

FINITE ELEMENT MODEL

The FE analyses are performed using the FE software Abaqus/Explicit 6.10-EF-1. Taking the advantage of symmetry, only a half-circular soil domain of diameter 42 m (=14*D*) and depth 20 m (=3.33*L*) is modeled as shown in Fig. 2. The size of the soil domain is large enough compared to the size of the caisson, and therefore, boundary effects are not found on calculated load, displacement and deformation mechanisms. Achmus et al. (2013) suggested that the diameter of the soil domain greater than 6.67D is sufficient. However, in the present study it is found that it depends upon the direction and location of loading and also on soil strength parameters. Therefore, a larger soil domain is used in this study to avoid any boundary effect. Note that the increase in size of the soil domain does not increase computational cost significantly because the size of the mesh is increased with distance from the caisson (Fig. 2).

In the FE model (Fig. 2), the vertical plane of symmetry is restrained from any displacement perpendicular to it, while the curved vertical surface of the soil domain is restrained from any lateral displacement using roller supports at the nodes. The bottom boundary is restrained from any vertical displacement, while the top boundary is free to displace.

The soil and the caisson are modeled using the C3D8R solid homogeneous elements available in Abaqus/Explicit element library, which are 8-noded linear brick elements with reduced integration and hourglass control. The mooring line is modeled as 3D wire using T3D2 element (a 2-node linear 3D truss element) with no interaction with soil domain. Typical FE mesh used in this study is shown in Fig. 2.

Modeling of Suction Caisson

A caisson of 6 m length, 3 m diameter and 100 mm wall thickness is modeled first. This geometry is referred as "base case" in the following sections. Analyses are also performed for different lengths and diameters to show the effects of aspect ratio. In the following sections, the results of base case are presented first. By modeling the caisson as elastic-perfectly plastic material and also as rigid body, it is found that the pullout capacity and rotation do not very significantly with these modeling techniques. However, the FE model with the caisson as a rigid body is computationally very efficient. Therefore, the caisson is considered as a rigid body in the FE analyses presented in the following sections.

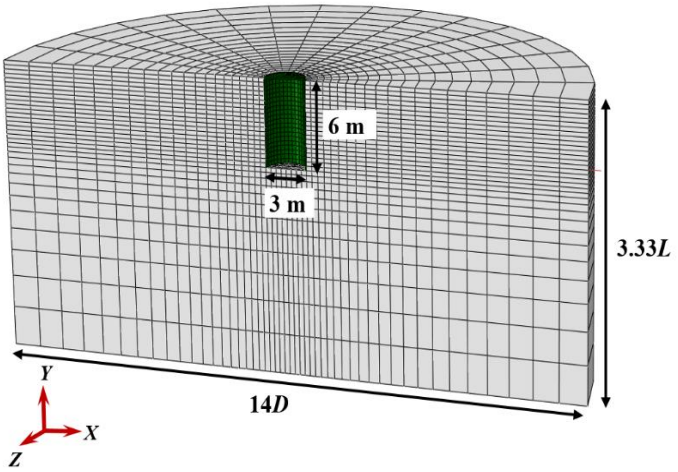

Fig. 2. Finite element mesh used in analysis

Modeling of Mooring Line

A wire of 50 m length and 100 mm diameter representing the mooring line connected to the suction caisson is modeled using truss elements with material properties of steel. The interface friction between the mooring line and soil is assumed to be zero. The pullout force is applied by a displacement boundary condition at the far end. However, all the results presented in the following sections are in terms of displacement of the padeye location.

Modeling of Sand

The sand is modeled using the built-in Mohr-Coulomb model available in the Abaqus FE software. The submerged unit weight of sand of 8.2 kN/m^3 is used. The geometry and mechanical properties used in the analysis are shown in Table 1. The dimension of the caisson for the base case analysis is similar to Bang et al. (2011). The soil parameters are estimated based on the soil properties mentioned in that study.

Interface Behavior

The soil/caisson interaction is modeled using the Coulomb friction model, which defines the friction coefficient (μ) as $\mu=\tan(\phi_\mu)$, where ϕ_μ is the soil/caisson interface friction angle. The value of ϕ_μ/ϕ' varies between 0 and 1 depending upon surface roughness, mean particle size of sand and method of installation (CFEM, 2006; Tiwari et al. 2010). For smooth steel pipe piles, ϕ_μ/ϕ is in the range of 0.5–0.7 (Potyondy,

1961; Coduto, 2001; Tiwari and Al-Adhadh, 2014)). For numerical modeling, ϕ_μ/ϕ' within this range has been also used in the past (e.g. Achmus et al. 2013). In the present study, $\phi_\mu=0.6\phi'$ is used. Authors understand that the axial resistance is significantly influenced by the factor. However, the pullout capacity is not significantly influenced by ϕ_μ/ϕ' for typical loading conditions in suction caisson.

Modulus of Elasticity of Sand

The Young's modulus of sand (E_s) can be expressed as a function of mean effective stress, p' as, $E_s=Kp_{atm}\left(p/p_{atm}\right)^n$ (Hardin and Black, 1966; Janbu 1963); where, K and n are two material parameters, p_{atm} is the atmospheric pressure (=100 kPa). However, in this study, no attempt has been taken to vary E_s with p', rather a constant value of E_s= 60 MPa is used.

Mooring Positions and Load Inclination Angles

The effects of mooring position and angle of loading are investigated for the base case parameters listed in Table 1. The loads are applied at 5%, 25%, 50%, 75% and 95% mooring positions from the top of the caisson. The inclination angle of the load (θ) is varied as 0°, 22.5°, 45°, 67.5° and 90° for each mooring position. That means, a total of 25 analyses are conducted for the base case to evaluate the effects of mooring position and load inclination angle.

Table 1. Geometry and mechanical properties in FE modeling

Suction Caisson	Outer diameter (D)	3 m
	Length (L)	6 m
Mooring Line	Modulus of elasticity (E_p)	2.08×10^8 kN/m^2
	Poisson's ratio (ν_p)	0.29
Sand	Angle of internal friction (ϕ')	39°
	Angle of dilation (ψ)	9°
	Young' modulus (E_s)	60,000 kN/m^2
	Poisson's ratio (ν_s)	0.30
	Cohesion (c')[1]	0.10 kN/m^2
	Submerged unit weight (γ')	8.2 kN/m^3

[1]Small cohesion is required to be defined in Abaqus FE analysis. For sand, in this study a very small value of c'=0.10 kN/m^2 is used.

RESULTS

Mesh Sensitivity Analysis

In general, smaller FE mesh yields more accurate results but computationally expensive. For efficient modeling, small elements are used near the caisson. The size of the elements is increased with increase in radial distance from the caisson as shown in Fig. 2. Similarly, the element size is increased with distance from the bottom of the caisson. To select the optimum mesh, several trial analyses are conducted with different mesh sizes. The force-displacement curves for three different sizes of mesh are shown Fig. 3 for 50% mooring position and loading angle, θ=0°. As shown in Fig. 3 that the calculated pullout force is smaller with fine mesh than that of with coarse mesh. In this study, the medium dense mesh is selected to perform the analyses as it is computationally faster, although it is recognized that it gives slightly higher pullout force than that of with fine mesh.

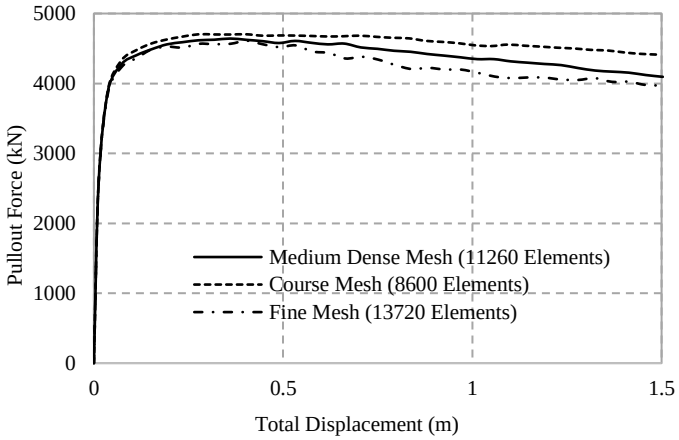

Fig. 3. Mesh Sensitivity Analysis

Force-displacement Curves

The variation of pullout force with total displacement along the direction of pulling is shown in Figs. 4 to 8 for different mooring positions. The pullout force is obtained from the axial force in the wire (truss element in this case). As Abaqus/Explicit is used, a large displacement could be applied without numerical issues. In this study, a total displacement of 1.5 m is applied.

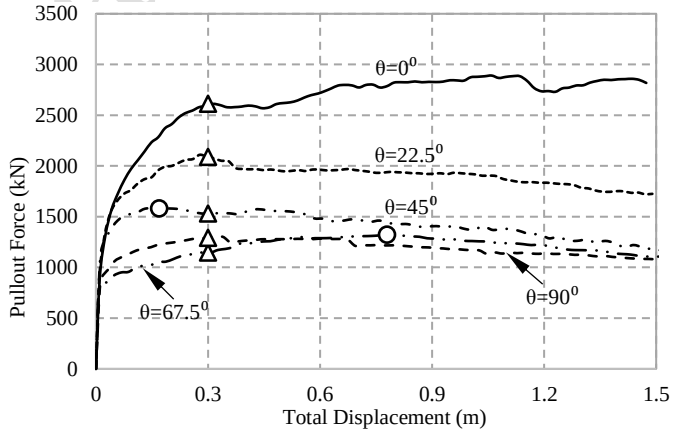

Fig. 4. Force-displacement curve for 5% mooring position

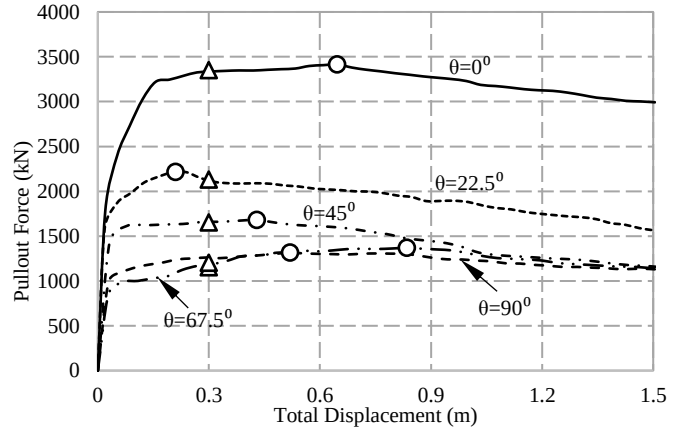

Fig. 5. Force-displacement curve for 25% mooring position

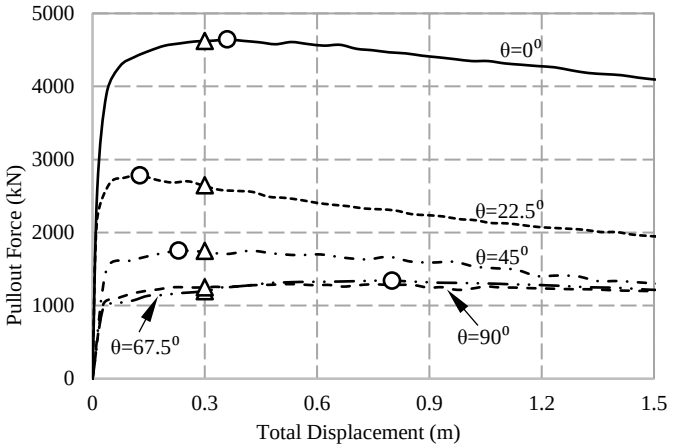

Fig. 6. Force-displacement curve for 50% mooring position

Several methods are available in the literature to estimate the maximum resistance or capacity of pipelines, anchors or pile foundations from force-displacement curves. As shown in Figs. 4 to 8, mainly four types of force-displacement curves are obtained from the present FE analyses. Firstly, the force-displacement curve does not show any clear peak as shown for θ=0° in Figs. 4 and 8. In this cases, the pullout force at 0.3 m (=0.1D) displacement is considered as the pullout capacity as shown by the open triangles in Figs. 4 and 8. The second type of force-displacement curve shows a clear peak at about $0.1D$ displacement as shown in Fig. 4 for θ=22.5°.

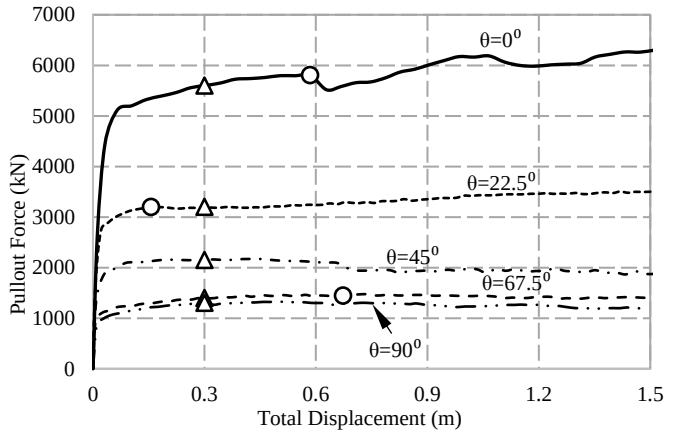

Fig. 7. Force-displacement curve for 75% mooring position

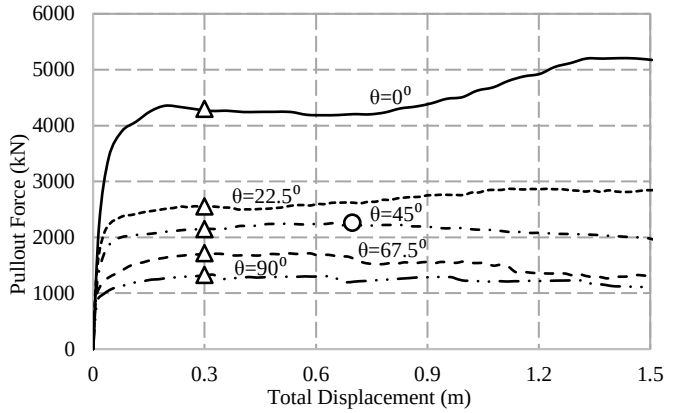

Fig. 8. Force-displacement curve for 95% mooring position

In the third type of force-displacement curves, a clear peak is formed before $0.1D$ displacement as shown in Fig. 4 for θ=45° and in Figs. 5 and 6 for θ=22.5° with open circles. Finally, in the fourth type the peak force is developed at displacements more than $0.1D$ as shown in Figs. 4 to 8 for θ=67.5° with open circles. However, it is found that in all cases the difference between the peak forces (circle) and the force at 0.1D displacement (triangle) is very small. Therefore, in this study the force at 0.1D displacement is considered as the pullout force. The decrease in pullout force at large displacement is mainly because of significant upward movement and rotation of the caisson at large displacement as discussed in the following sections.

Pullout Capacity

The pullout capacities for different loading angles and mooring positions are shown in Fig. 9. The lines with open symbols represents the FE results while the data points of same solid symbol show the centrifuge test results (Bang et al., 2011) of similar conditions. The pullout capacities obtained from the present FE analysis follow the similar trend as obtained in the centrifuge tests (Bang et al. 2011). For a given mooring position, the maximum pullout capacity is obtained for lateral loading (θ=0°), while the minimum pullout capacity is obtained for θ=90°. The difference between the pullout capacity for θ=90° and θ=67.5° is very small for mooring position up to 75%, because in these cases the caisson moves almost vertically. Note that, even at θ=90° the caisson does not move pure vertically as the padeye is located on one side of the caisson and therefore some counterclockwise rotation is occurred. The maximum pullout capacity is developed approximately at 75% mooring position for $\theta \leq 45°$.

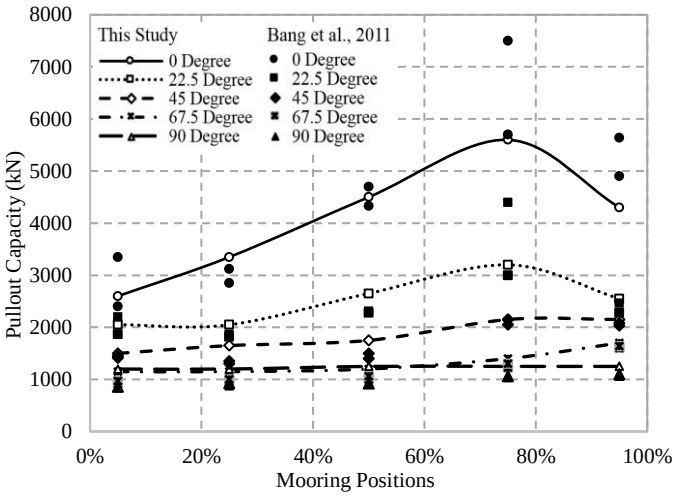

Fig. 9. Comparison of pullout capacity between FE and centrifuge tests

Rotation

The rotation of the caisson has a significant effect on force-displacement behavior. The rotation of the caisson about the geometric center with total displacement is plotted in Figs. 10 to 14 for different mooring positions and different load inclination angles. The sign convention used for rotations is shown in Fig. 1(c) in which positive value represents clockwise rotation. As shown in Fig. 10 for 5% mooring position, the caisson rotates clockwise for θ=0°, 22.5° and 45°. However, for θ=90° counterclockwise rotation is observed. For

θ=67.5°, very small rotation of the caisson is found. Similar trend is found for 25% and 50% mooring positions (Figs. 11 and 12). Opposite trend of rotation is noticed for 75% and 95% mooring positions (Figs. 13 and 14). In these cases, the caisson rotates in the counterclockwise direction.

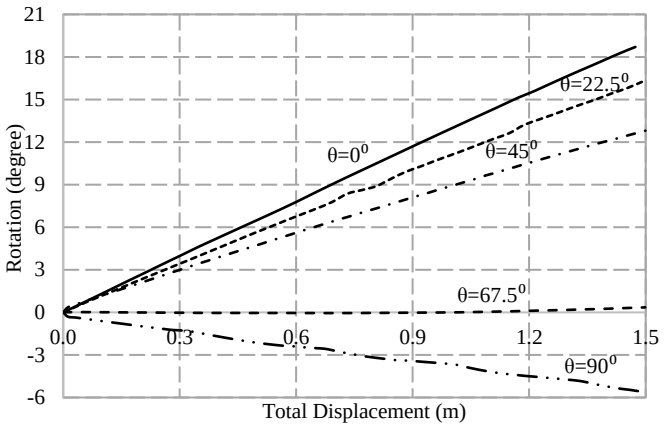

Fig. 10. Rotation-displacement curve for 5% mooring position

The rotation of the caisson with pullout force is plotted in Figs. 15 to 19. As shown in Figs. 15 to 17 that the maximum clockwise rotation (+ve) is occurred for θ=0° at 5%, 25% and 50% mooring positions. The rotation is decreased with increase in θ and becomes negative (counter clockwise) for θ=67.5° and 90°. On the other hand, rotation is negative for all θ at 75% and 95% mooring positions (Figs. 18 and 19). The pattern of rotation obtained from the present FE analyses is very similar to model test results of Gao et al. (2013). The open triangles in Figs. 15 to 19 show the pullout capacity (0.1*D* displacement). As shown, the rotation of the caisson is significantly different at the pullout capacity for different values of θ and mooring positions.

The rotation of the caisson at the pullout capacity (0.1*D* displacement) is shown in Fig. 20 for different mooring positions and load inclination angles. The clockwise positive rotation is occurred for 5%, 25% and 50% mooring positions for θ=0°, 22.5° and 45°. The maximum positive rotation is occurred for 50% mooring position at θ=0°. On the other hand, counterclockwise (negative) rotation is occurred for 75% and 95% mooring positions. Very small rotation is calculated for large values of θ (=67.5° and 90°), which is also almost independent of mooring position. This is one of the reasons of calculating similar pullout capacity at these loading angles as shown in Fig. 9.

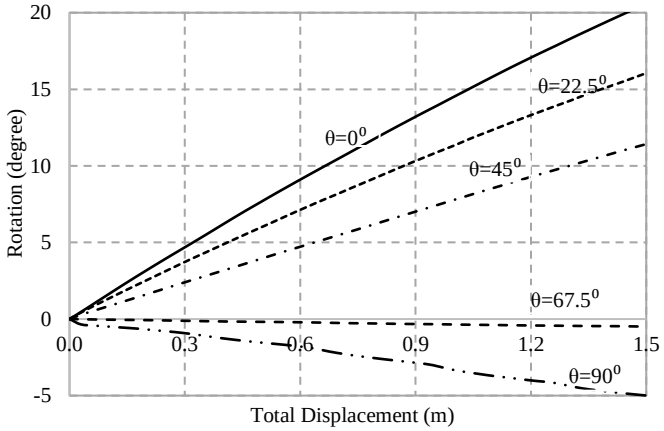

Fig. 11. Rotation-displacement curve for 25% mooring position

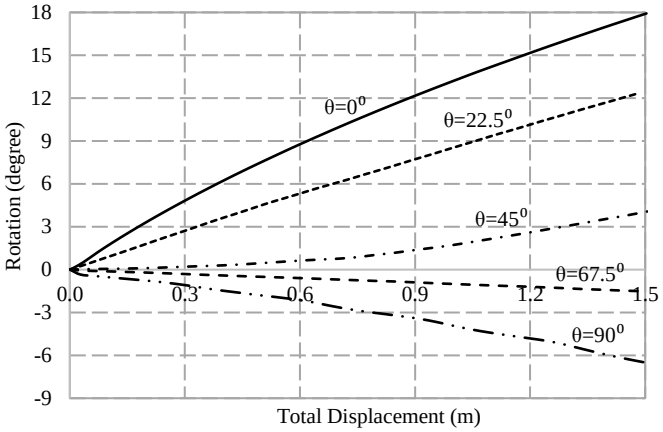

Fig. 12. Rotation-displacement curve for 50% mooring position

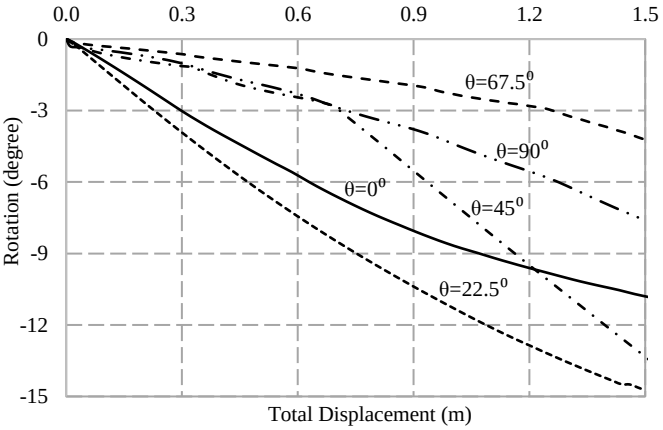

Fig. 13. Rotation-displacement curve for 75% mooring position

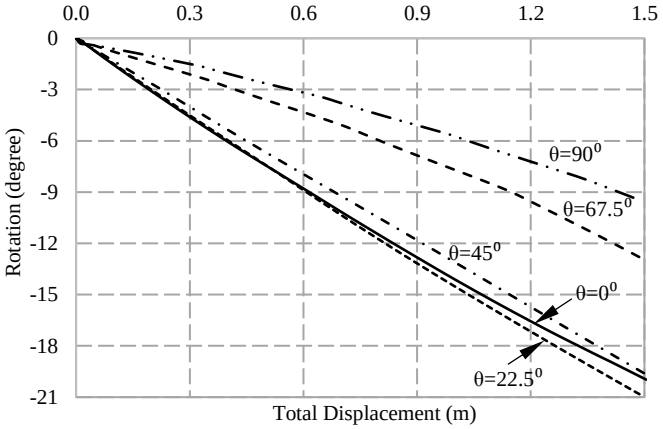

Fig. 14. Rotation-displacement curve for 95% mooring position

Lateral Displacement

Fig. 21 shows the lateral displacement of the geometric centerline of the caisson with depth for different mooring positions at θ=0° at the pullout capacity (0.1*D* displacement). The lateral displacements for loading at 5%, 25% and 50% mooring positions are opposite to that of 75% and 95% mooring positions. The minimum lateral displacement and rotation of the caisson are occurred for loading at θ=0° and 75% mooring position.

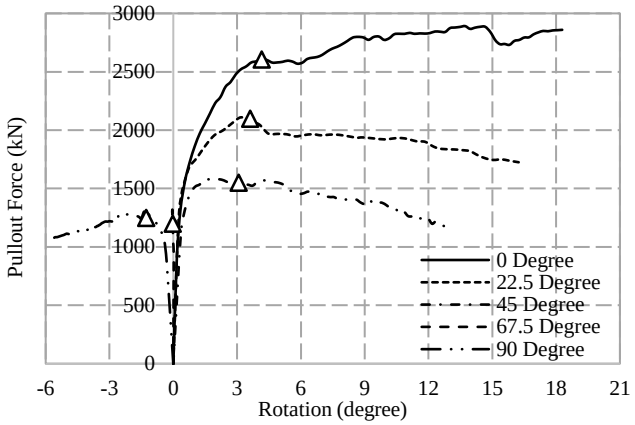

Fig. 15. Force-rotation curve for 5% mooring position

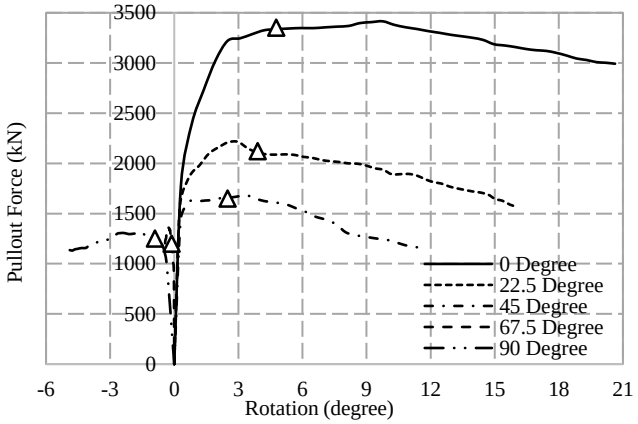

Fig. 16. Force-rotation curve for 25% mooring position

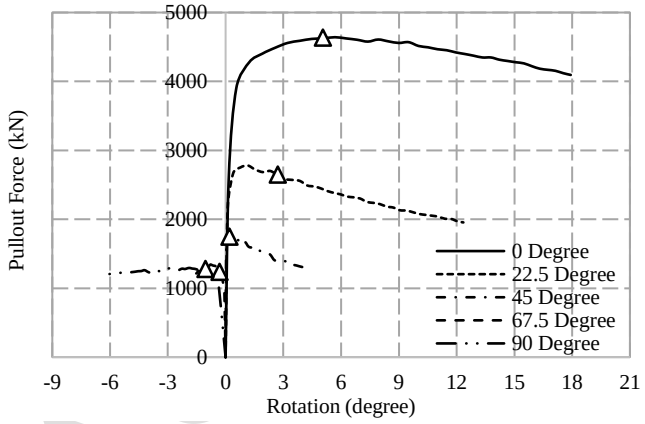

Fig. 17. Force-rotation curve for 50% mooring position

Shape of Soil Failure Wedge

The shape of failure wedge of soil due to inclined loading applied on the caisson is dependent on mooring position and loading angle. The maximum principal plastic strain and the magnitude of total displacements for loading at 25% and 75% mooring positions at θ=0° are shown in Fig. 22 and Fig. 23, respectively. As shown in Fig. 22(a) that significant plastic strain develops in a narrow zone in the right side of the caisson, and a wedge of soil is pushed upward forming heave in the right side of the caisson. The plastic strain inside the wedge is not very significant. The movement of this wedge is governed by the passive resistance of the soil. In the left side, a gap is formed near the bottom of the caisson and a wedge of soil moves downward resulting in settlement at the seabed. This gap is possibly due to the very low value of cohesion used in the FE analyses. The failure of this soil wedge is mainly governed by the active failure condition.

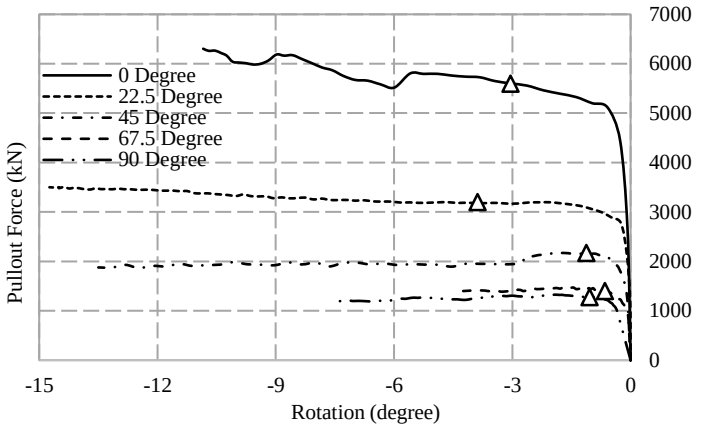

Fig. 18. Force-rotation curve for 75% mooring position

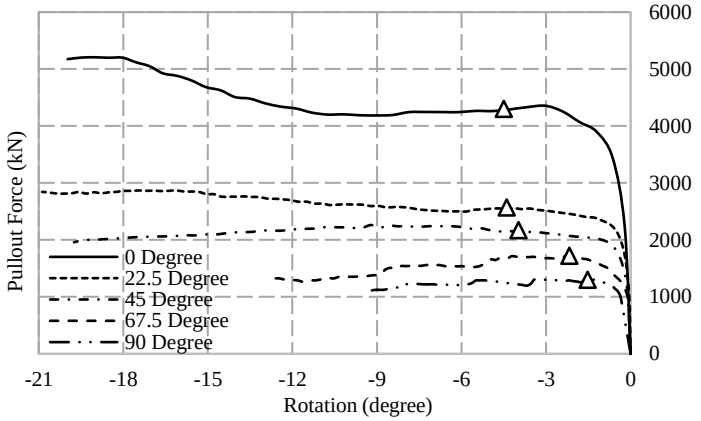

Fig. 19. Force-rotation curve for 95% mooring position

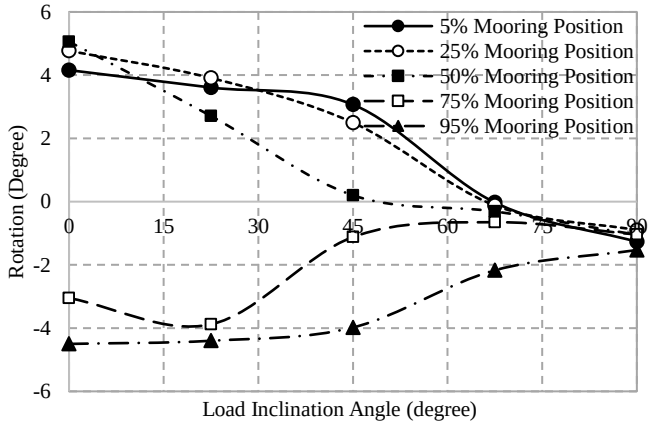

Fig. 20. Rotation of caisson at pullout capacity

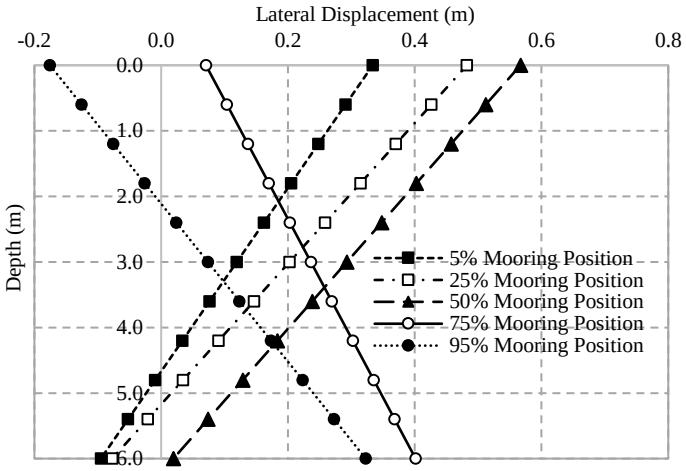

Fig. 21. Lateral displacement of caisson for θ=0°

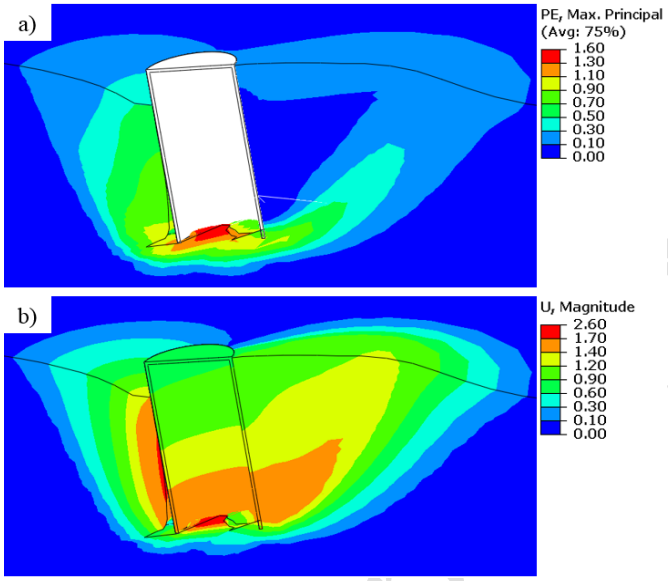

Fig. 22. Maximum principal plastic strain and total displacement profile for 75% mooring position and 1.5 m displacement at θ=0°

When the caisson is loaded at 25% mooring position, the rotation is in the opposite direction of the rotation for 75% mooring position. Therefore, the soil failure pattern is different as shown in Fig. 23. The formation of failure wedge in the *xy* plane for different mooring positions and loading angles obtained from the present FE analyses are shown schematically in Figs. 24 and 25. When the caisson is loaded at θ=67.5° and θ=90° the caisson rotates counterclockwise and failure wedges as shown in Fig. 24 is formed irrespective of the mooring positions. On the other hand, when the caisson is loaded at θ=0°, 22.5° and 45°, the failure pattern depends on mooring position because of the rotation of the caisson in different direction (Fig. 25). When the caisson is loaded at 5%, 25% and 50% mooring positions, the failure wedge shown in Fig. 25(a) is formed. However, when it is loaded at 75% and 95% mooring position, a larger passive wedge is formed as shown in Fig. 25(b). This important phenomenon should be considered in the calculation of the pullout capacity of the caisson.

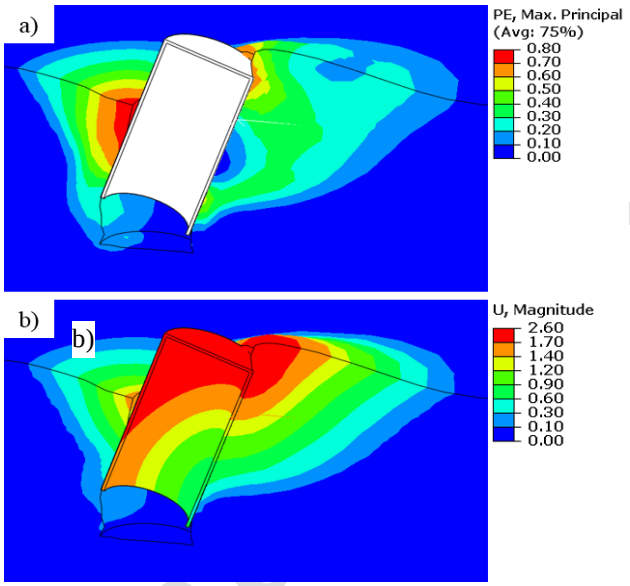

Fig. 23. Maximum principal plastic strain and total displacement profile for 25% mooring position and 1.5 m displacement at θ=0°

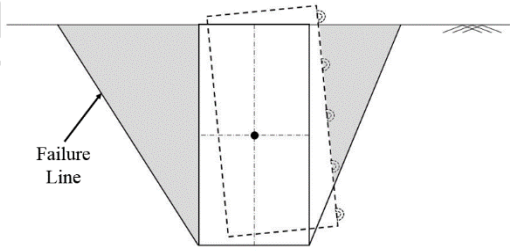

Fig. 24. Failure wedge for θ=67.5° and 90° and all mooring positions

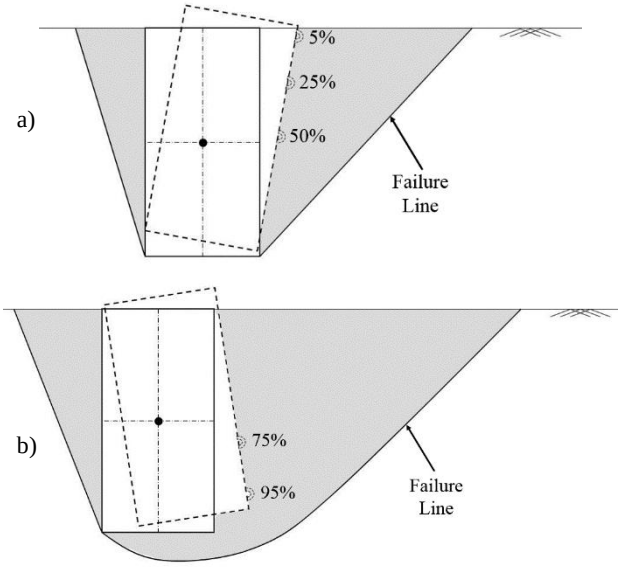

Fig. 25. Failure wedge for θ=0°, 22.5° and 45°: (a) mooring position 5%, 25% and 50%, (b) mooring position 75% and 95%

EFFECT OF ASPECT RATIO (*L*/*D*)

The results presented in the previous sections are for the base case, where length *L*=6 m and diameter *D*=3 m is used. In this section, the pullout capacity for different *L*/*D* ratio is presented. A total of 35 additional analyses are performed to investigate the effect of *L*/*D* ratio on pullout capacity. The dimensions of the caisson are listed in Table 2. All the analyses are conducted for 5%, 25%, 50%, 75% and 95% mooring positions. Only one value of θ (=0°) is used and the results are compared with the centrifuge tests results by Jang and Kim (2013) where the applied load was in the lateral direction. The soil parameters used in the analysis are listed in Table 1. Typical force-displacement curve for 50% mooring position with different *L*/*D* ratio is shown in Fig. 26. The pullout force and displacement are normalized as Deng and Carter (2000), where σ'_v is the initial vertical effective stress at the bottom of the caisson. The normalization with σ'_v is required because the shear strength of sand depends on effective stress, and for a given *L*/*D* ratio, σ'_v is higher for larger diameter caissons than that of smaller diameters. As shown in Fig. 26, the normalized pullout force increases with increase in *L*/*D* ratio, and for a given *L*/*D* ratio, the normalized force is slightly higher for *L*=6 m than that of for *L*=9 m.

Table 2. Geometric parameters for different aspect ratios

L/*D*	*L* (m)	*D* (m)	*L* (m)	*D* (m)
1.5	9	6	6	4
2.0	9	4.5	6	3
2.5	9	3.6	6	2.4
3.0	9	3	6	2

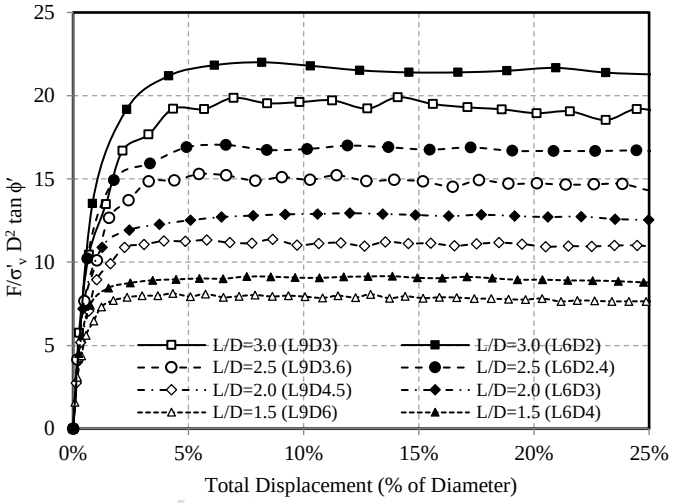

Fig. 26. Normalized Force-displacement curves for 50% mooring position

The normalized pullout capacity for different mooring position is shown in Fig. 27. For all four *L*/*D* ratio, the maximum pullout force is obtained for 75% mooring position. Although limited, the centrifuge test results of Jang and Kim (2013) are also shown in Fig. 27. The present FE results compare well the centrifuge test results.

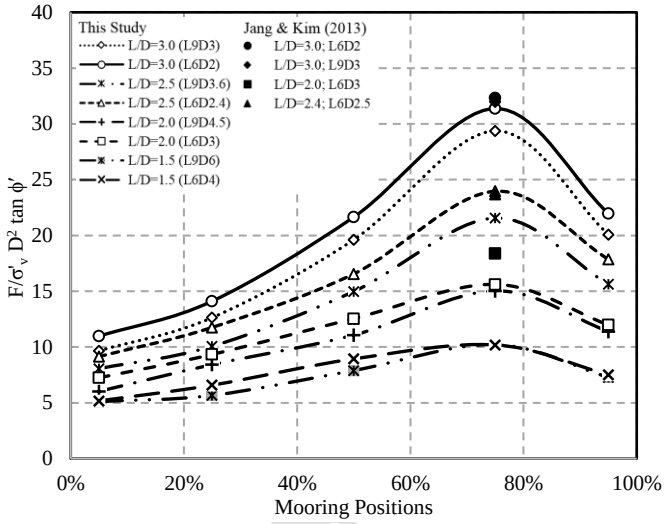

Fig. 27. Normalized pullout capacity for θ=0° for different mooring positions

ANALYSES USING MODIFIED MOHR-COULOMB MODEL

In the analyses presented in the previous section, the built-in Mohr-Coulomb model is used where constant values of ϕ′ and ψ are assigned. However, in laboratory test, dense sand shows post-peak softening behavior and the behavior of sand also depends on mode of shearing, such as triaxial (TX), direct shear (DS) or direct simple shear (DSS) conditions. In this section, FE analyses are performed using a modified Mohr-Coulomb (MMC) model (Roy et al. 2014a), where pre-peak hardening, post-peak softening, density and confining pressure dependent friction and dilation angles are considered. The key features of this model are:

i) The difference between angle of internal friction at the peak (ϕ'_p) and critical state (ϕ'_c) increases with increase in relative density (D_r) and reduction of confining pressure.

ii) The maximum dilation angle (ψ_p) can be calculated as $\psi_p = (\phi'_p - \phi'_c)/k_\psi$, where k_ψ is a soil parameter (Bolton, 1986).

iii) The angle of internal friction and dilation angle are not constant but varies with plastic shear strain γ^p. With increase in γ^p, the mobilized ϕ′ and ψ increase (i.e. hardening) up to the peak value and then decrease at large γ^p (softening).

All the above features of dense sand behavior have been modeled using a set of equations listed in Table 3. A detailed discussion of this model and its performance are available in Roy et al. (2014a & b). The MMC model has been implemented in Abaqus with the aid of a user-subroutine written in FORTRAN. The soil parameters used in the present analysis are: A_ψ=3.8, k_ψ=0.6, ϕ'_{in}=29°, C_1=0.22, C_2=0.11, m=0.25, ϕ'_c=31° and D_r=80%. The inset in Table 3 shows the variation of mobilized ϕ′ and ψ for these soil parameters for p'=50 kPa.

As mentioned before, constant values of ϕ′ and ψ are commonly used in the design of pile foundations. The American Petroleum Institute (API, 1987) recommended that ϕ′ (in degree) can be estimated as $\phi'=16D_r^2+0.17D_r+28.4$. For D_r=80%, ϕ′=39° is calculated. Now using ϕ′=39° and ψ=9° an analysis has been also performed using MC model. Figure 28 shows the pullout force for the base case caisson geometry loaded at 75% mooring position. For lower values of θ (≤45°) the pullout force is higher for the MC model that that of with the MMC model. The difference reduces with increase in θ. In order to explain the mechanisms, the plastic shear strains developed at 10% and 30%

padeye displacement for θ=0° are plotted in Fig. 29. Figure 29 shows that the size of passive failure wedge obtained by MC model is slightly larger than that obtained by MMC model, which is one of the contributory factors of higher pullout capacity by MC model (Fig. 26).

Figure 30 show the mobilized ϕ' and ψ at these padeye displacements for MMC model. As shown in the insets of Table 3 that the maximum ϕ' and ψ are mobilized at γ_p^p, and their values are less than the peak values in the pre-peak ($\gamma_p < \gamma_p^p$) and also in the post-peak ($\gamma_p > \gamma_p^p$) zones. The first column of Fig. 30 shows that, at 10% displacement, the post-peak condition is developed near the caisson (colored zone), while the gray zones represents the pre-peak shear zones where some plastic shear strains develop but less than γ_p^p. With increase in displacement, plastic shear strain increases along the failure plane that reduces the mobilized ϕ' and ψ to critical state. In other words, the mobilized ϕ' and ψ are not constant along the failure plane in the simulation with MMC. On the other hand, in the MC model they are constant (ϕ'=39° and ψ =9°).

From the above analyses it can be concluded that, although the force-displacement curves could be matched, the mobilized shear strength in the soil is different for MC and MMC model.

Table 3: Equations for Modified Mohr-Coulomb Model (MMC) (after Roy et al. 2014a)

Description	Constitutive Equation	Soil Parameters
Relative density index	$I_R = I_D(Q - \ln p') - R$	$I_D = D_r(\%)/100$, Q=10, R=1 (Bolton, 1986)
Peak friction angle	$\phi'_p - \phi'_c = A_\psi I_R$	ϕ'_c, A_ψ
Peak dilation angle	$\psi_p = \dfrac{\phi'_p - \phi'_c}{k_\psi}$	k_ψ
Strain softening parameter	$\gamma_c^p = C_1 - C_2 I_D$	C_1, C_2
Plastic strain at ϕ'_p	$\gamma_p^p = \gamma_c^p \left(p'/p'_a\right)^m$	p'_a, m
Mobilized friction angle at Zone-II	$\phi' = \phi'_{in} + \sin^{-1}\left[\left(\dfrac{2\sqrt{\gamma^p \gamma_p^p}}{\gamma^p + \gamma_p^p}\right)\sin\left(\phi'_p - \phi'_{in}\right)\right]$	
Mobilized dilation angle at Zone-II	$\psi = \sin^{-1}\left[\left(\dfrac{2\sqrt{\gamma^p \gamma_p^p}}{\gamma^p + \gamma_p^p}\right)\sin\left(\psi_p\right)\right]$	
Mobilized friction angle at Zone-III	$\phi' = \phi'_c + \left(\phi'_p - \phi'_c\right)\exp\left[-\left(\dfrac{\gamma^p - \gamma_p^p}{\gamma_c^p}\right)^2\right]$	
Mobilized dilation angle at Zone-III	$\psi = \psi_p \exp\left[-\left(\dfrac{\gamma^p - \gamma_p^p}{\gamma_c^p}\right)^2\right]$	

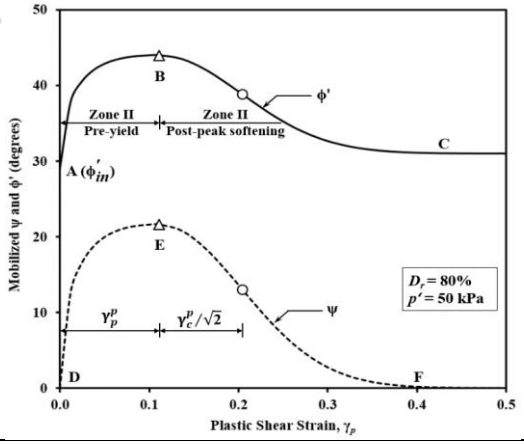

Symbols: A_ψ: slope of $(\phi'_p - \phi'_c)$ vs. I_R; m, C_1, C_2: soil parameters; I_R: relative density index; k_ψ: slope of $(\phi'_p - \phi'_c)$ vs. ψ_p; ϕ'_{in}: ϕ' at the start of plastic deformation; ϕ'_p: peak friction angle; ϕ'_c: critical state friction angle; ψ_p: peak dilation angle; ψ_{in}: ψ at the start of plastic deformation (=0); γ^p: engineering plastic shear strain; γ_p^p: γ^p required to mobilize ϕ'_p; γ_c^p: strain softening parameter

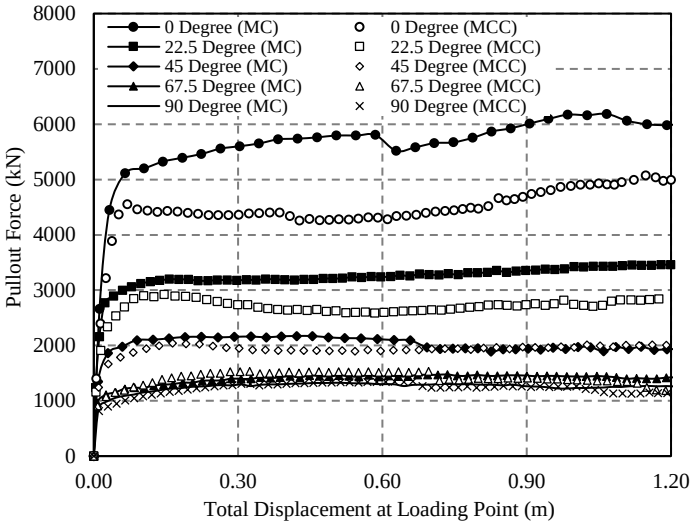

Figure 28. Force-displacement curve for 75% mooring position with MC and MMC model

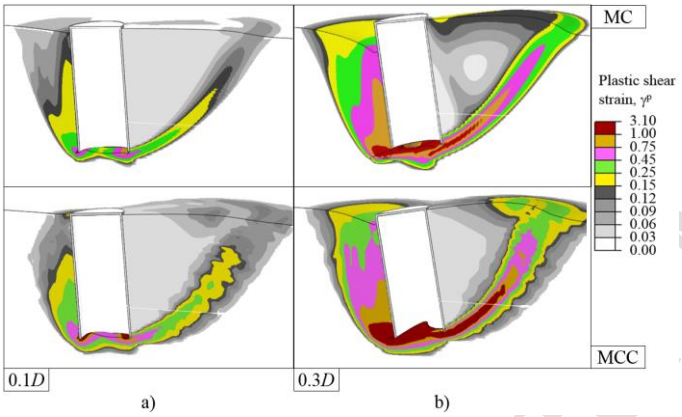

Fig. 29. Development of plastic shear strain at 0.1*D* and 0.3*D* padeye displacement

CONCLUSIONS

A comprehensive three-dimensional FE analyses are performed to investigate the response of suction caissons in dense sand subjected to oblique loading. The analyses are performed using Abaqus/Explicit FE software. The effects of constitutive behavior of sand on pullout capacity are examined using two soil constitutive models. In the first set of analyses, the built-in elastic perfectly plastic Mohr-Coulomb (MC) model in Abaqus is used. The second set analyses are conducted to capture the pre-peak hardening, post-peak softening, and effects of density and confining pressure on stress-strain behavior of dense sand by employing a modified form of Mohr-Coulomb model (MMC) with the aid of a user-subroutine. Large displacements are applied to examine the effects of rotation of the caisson on pullout force. The results obtained from the present FE analyses compare well with available centrifuge test results. The pullout capacity is also examined for three key factors: mooring position, load inclination angle and *L*/*D* ratio.

When MC model is used, the pullout force at 0.1*D* can be used as pullout capacity for the cases analyzed. The pullout force decreases at large displacement except for θ=0°. The upward movement and rotation of the caisson are the cause of the reduction of force. The rotation of the caisson at the pullout capacity varies with θ and mooring position. The rotation has a significant effect on pullout capacity. The failure wedge formed due to displacement of the caisson is a function of θ and mooring position. The maximum pullout capacity is obtained for 75% mooring position at θ=0°. Moreover, the increase of *L*/*D* ratio increases the normalized pullout capacity.

For the MMC model, the pullout force is slightly lower than that of MC model, and the difference between these two is higher for low load angles. Noticeable post-peak degradation is found for θ≤45°. Even though the force displacement curves could be matched, the mobilized ϕ′ and ψ are different in MC and MMC models along the failure plane.

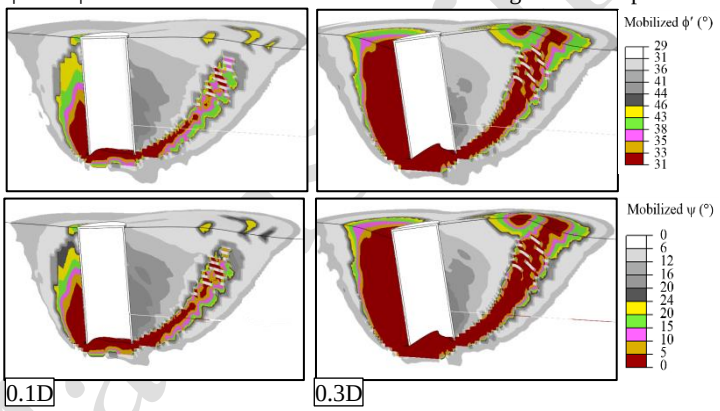

Fig. 30. Mobilized ϕ′ and ψ using MMC for 0.1*D* and 0.3*D* padeye displacement

ACKNOWLEDGEMENTS

The work presented in this paper has been funded by NSERC Discovery grant, MITACS and Petroleum Research Newfoundland & Labrador (PRNL). Authors express their thanks to Md. Iftekharuzzaman and Kshama Roy for their help with FE model development.

REFERENCES

Achmus, M, Akdag, CT and Thieken, K (2013). "Load-bearing behavior of suction bucket foundations in sand," *Applied Ocean Research*, Vol. 43, pp. 157-165.

Allersma, HGB, Brinkgreve, RBJ, Simon, T and Kirstein, AA (2000). "Centrifuge and Numerical Modelling of Horizontally Loaded Suction Piles," *International Journal of Offshore and Polar Engineering*, Vol. 10, No. 3, pp. 222-228.

API (1987). "Recommended practice for planning, designing and constructing fixed offshore platforms," API *Recommended practice 2A (RP2A)*, 17th ed., American Petroleum Institute.

Aubeny, CP, Han SW and Murff, JD (2003). "Inclined load capacity of suction caissons," *International Journal for Numerical and Analytical Methods in Geomechanics*, Vol. 27, pp. 1235-1254.

Bang, S, Jones, KD, Kim, KO, Kim, YS and Cho, Y (2011). "Inclined loading capacity of suction piles in sand," *Journal of Ocean Engineering*, Vol. 38, pp. 915-924.

Bolton, MD (1986). "The strength and dilatancy of sand," *Géotechnique*, Vol. 36, No. 1, pp. 65-78.

Cao, J, Phillips, R, Audibert, JME and Al-Khafazi, Z (2002b). "Numerical analysis of the behavior of suction caissons in clay," *Proceedings of the 12th International Offshore and Polar Engineering Conference*, Kitakyushu, Japan, May 26-31, pp. 795-799.

Cao, J, Phillips, R, Popescu, R, Al-Khafaji, Z, and Audibert, JME (2002a). "Penetration resistance of suction caissons in clay," *Proceedings of the 12th International Offshore and Polar Engineering Conference*, Kitakyushu, May 26-31, pp. 800-806.

Cao, J, Phillips, R, Popescu, R, Audibert, JME and Al-Khafaji, Z (2003). "Numerical analysis of the behavior of suction caissons in clay," *International Journal of Offshore and Polar Engineering*, Vol. 13, No. 2, pp. 154-159.

CFEM (2006). "Canadian Foundation Engineering Manual," 4th ed., *Canadian Geotechnical Society*, Richmond, BC, Canada.

Coduto, DP (2011). *Foundation design: Principles & practices*, 2nd ed., Prentice Hall, Upper Saddle River, New Jersey, United States.

Deng, W, and Carter, JP (2000). "Inclined uplift capacity of suction caissons in sand," *Offshore Technology Conference*, Houston, Texas, OTC 12196, pp. 809-820.

Gao, Y, Qiu, Y, Li, B, Li, D, Sha, C and Zheng, X (2013). "Experimental studies on the anti-uplift behavior of the suction caissons in sand," *Applied Ocean Research*, Vol. 43, pp. 37-45.

Handayanu, Swamidas ASJ, Booton M (2000). "Ultimate strength of offshore tension foundations under vertical and inclined loads," *Proc. of the International Conference on Offshore Mechanics and Arctic Engineering*, New Orleans, Louisiana, Vol. 2, pp. 95-100.

Hardin, BO and Black, WL (1966). "Sand stiffness under various triaxial stresses," *Journal of the Soil Mechanics and Foundations Division*, Vol. 92, No. 2, pp. 27-42.

Houlsby, GT and Byrne, BW (2005a). "Calculation procedures for installation of suction caissons in sand," *Proc ICE - Geotechnical Engineering*, Vol. 158, No 3, pp. 135-144.

Houlsby, GT and Byrne, BW (2005b). "Calculation procedures for installation of suction caissons in clay and other soils," *Proc ICE - Geotechnical Engineering*, Vol. 158, No 2, pp. 75-82.

Iftekharuzzaman, Md and Hawlader, B (2012). "Numerical modeling of pullout capacity of a suction pile in sand under oblique load," *Second International Conference on Geotechnique, Construction Materials and Environment*, Kuala Lumpur, Malaysia, Nov. pp. 14-16.

Janbu, N (1963). "Soil Compressibility As Determined By Oedometer And Triaxial Test," *Proceedings of 3rd European Conference on Soil Mechanics and Foundation Engineering*, Wiesbaden, Germany, Vol. 1, pp. 19-25.

Jang, YS and Kim, YS (2013). "Centrifugal Model Behavior of Laterally Loaded Suction Pile in Sand," *KSCE Journal of Civil Engineering*, Vol. 17, No. 5, pp. 980-988.

Jones, KD, Bang, S and Cho, Y (2007). "Pullout capacity of embedded suction anchors in sand," *Journal of Ocean Engineering*, Vol. 34, Issue 16, pp. 2107–2114.

Kim, KO, Kim, YS, Cho, Y, Bang, S and Jones, K (2009). "Centrifuge Model Tests on Suction Piles in Sand under Inclined Loading," *Proceedings of the Nineteenth International Offshore and Polar Engineering Conference*, Osaka, Japan, June 21-26, Vol. II, pp.191-196.

Kim, Y, Kim, K, Cho, Y and Bang, S (2010). "Centrifuge model tests on suction pile pullout loading capacity in sand," *Int. Conf. on Physical Modelling in Geomechanics*, Vol. 2, pp. 787-792.

Kim, YS, Kim, KO, Cho, Y, Bang, S and Jones, K (2005). "Centrifuge Model Tests on Embedded Suction Anchors," *Proceedings of the Fifteenth International Offshore and Polar Engineering Conference*, Seoul, Korea, June 19-24, Vol. II, pp.431-435.

Lee, SH, Cho, Y, Kim, KO, Kim, YS, Lee, TH, and Kwag, DJ (2003). "Centrifuge model tests on embedded suction anchor loading capacities," *Proceedings of The Thirteenth International Offshore and Polar Engineering Conference*, Honolulu, Hawaii, USA, May 25−30, Vol. II, pp. 789-793.

Potyondy, JG (1961). "Skin friction between various soils and construction materials," *Géotechnique*, Vol. 11, No. 4, pp. 339–353.

Roy, K, Hawlader, B and Kenny, S (2014a). "Influence of Low Confining Pressure in Modeling of Lateral Pipeline/Soil Interaction in Dense Sand," *Proceedings of the ASME 2014 33rd International Conference on Ocean, Offshore and Arctic Engineering*, San Francisco, California, USA, June 8–13, pp. V06BT04A050.

Roy, K, Hawlader, B, Kenny, S and Moore, I (2014b). "Finite element modeling of uplift pipeline/soil interaction in dense sand," *Geohazards6*, Kingston, Ontario, Canada, June 15–18.

Sukumaran, B, McCarron, WO, Jeanjean, P and Abouseeda, H (1999). "Efficient finite element techniques for limit analysis of suction caissons under lateral loads," *Computers and Geotechnics*, Vol. 24, pp. 89-107.

Tiwari, B and Al-Adhadh, AR (2014). "Influence of Relative Density on Static Soil–Structure Frictional Resistance of Dry and Saturated Sand," *Geotechnical and Geological Engineering*, Vol. 32, pp. 411–427.

Tiwari, B, Ajmera, B and Kaya, G (2010). "Shear strength reduction at soil–structure interaction," *GeoFlorida 2010: Advances in Analysis, Modeling & Design*, Orlando, Florida, United States, February 20-24, pp. 1747–1756.

Tran, MN, Randolph, MF and Airey, DW (2007). "Installation of suction caissons in sand with silt layers," *Journal of Geotechnical and Geoenvironmental Engineering*, Vol. 133, No. 10, pp. 1183-1191.

Zdravkovic, L, Potts, DM, and Jardine, RJ (2001). "A parametric study of the pull-out capacity of bucket foundations in soft clay," *Géotechnique*, Vol. 51, No. 1, pp. 55-67.